

Impact of Regional SST Anomalies on the Indian Monsoon Response to Global Warming in the CNRM Climate Model

H. DOUVILLE

Météo-France/CNRM, Toulouse, France

(Manuscript received 20 July 2004, in final form 12 October 2005)

ABSTRACT

While transient climate change experiments with coupled atmosphere–ocean general circulation models undoubtedly represent the most comprehensive tool for studying the climate response to increasing concentrations of greenhouse gases (GHGs), less computationally expensive time-slice experiments with atmospheric GCMs are still useful to test the robustness of the projected climate change. In the present study, three sets of time-slice experiments with prescribed sea surface temperature (SST) are compared to a reference climate scenario obtained with the Centre National de Recherches Météorologiques Coupled Climate Model (CCM). The main objective is to assess the sensitivity of the monsoon response to the magnitude or pattern of SST anomalies in two regions where such anomalies are highly model dependent, namely, the circumpolar Southern Ocean and the tropical Pacific Ocean. On the one hand, it is shown that the regional climate anomalies predicted by the CCM can be reproduced at least qualitatively by a pair of time-slice experiments in which the present-day SST biases of the CCM are removed. On the other hand, the results indicate that the Indian monsoon response to increasing amounts of GHG is sensitive to regional uncertainties in the prescribed SST warming. Increasing the sea surface warming in the southern high latitudes to compensate for the weak sea ice feedback simulated by the CCM around the Antarctic has a significant influence on the regional climate change simulated over India, through a perturbation of the regional Hadley circulation. Prescribing zonal mean rather than El Niño-like SST anomalies in the tropical Pacific has an even stronger impact on the monsoon response, through a modification of the Walker circulation. These results suggest that both deficiencies in simulating present-day climate (even at high latitudes) and uncertainties in the SST patterns caused by enhanced GHG concentrations (especially in the tropical Pacific) are major obstacles for predicting climate change at the regional scale.

1. Introduction

Though the Indian summer monsoon rainfall shows little significant trend over the entire twentieth century (Rupa Kumar et al. 1992; Pant and Rupa Kumar 1997), the perspective of a possible impact of global warming on the Indian subcontinent remains a major issue for the large population of this region. Given the extreme dependence of Indian water resources on the summer rainy season, even a moderate decrease in monsoon intensity could have serious consequences on the economy. Moreover, possible impacts on climate variability could also lead to an increased risk of floods and/or droughts.

Unfortunately, numerical climate projections based on coupled atmosphere–ocean GCMs are still very uncertain at the regional scale, especially where precipitation is concerned. While a majority of studies (see, e.g., Meehl and Washington 1993; Hu et al. 2000; Rupa Kumar and Ashrit 2001) indicate a significant increase in monsoon rainfall with increasing amounts of greenhouse gases (GHGs), the regional distribution of the precipitation anomalies over the Indian peninsula remain highly model dependent. Even on the continental scale, changes in all-India rainfall remain very uncertain (Lal et al. 1994, 1995; Mitchell and Johns 1997; Douville et al. 2000a,b).

Clearly, there are so many uncertainties both in the emission scenarios and the models themselves, that multimodel ensembles of climate scenarios are necessary to achieve a more reliable assessment of the potential impacts of human activities on regional climates. However, coupled atmosphere–ocean GCMs

Corresponding author address: Dr. Hervé Douville, CNRM/GMGEC/UDC, 42 avenue Coriolis, 31057 Toulouse Cedex 01, France.
E-mail: herve.douville@meteo.fr

(AOGCMs) are still computationally expensive and transient climate change experiments cannot be run as often as necessary to explore all sources of uncertainty in future climate projections. To overcome this difficulty, time-slice atmospheric experiments have been used for many years, and even before the availability of global coupled AOGCMs. Such experiments are aimed at simulating the equilibrium response of the atmosphere to enhanced concentrations of GHG. While early studies assumed a homogeneous warming of SST, the SST boundary conditions are now derived from coupled ocean–atmosphere scenarios, at two intervals corresponding to the present-day and future climate, respectively. Such atmospheric simulations are much less computationally expensive than coupled integrations and have been shown to capture the qualitative response of the reference climate scenario (Stephenson and Held 1993). Therefore, they allow modelers to multiply the number of climate change simulations, and thereby to assess the relevance of various uncertainties in their climate scenarios.

In the present study, the response of the Indian summer monsoon to increasing amounts of GHG and sulfate aerosols is compared between a reference climate scenario and three sets of time-slice experiments. The reference scenario, SG1, was performed with the Action de Recherche Petite Echelle Grande Echelle–Océan Parallélisé (ARPEGE–OPA) coupled AOGCM and was described in detail by Ashrit et al. (2003). The mean model response in the second half of the twenty-first century indicates a significant increase in the annual mean surface air temperature (about 2°C) and in monsoon precipitation (less than 10%) over India, relative to the 1950–99 climatology. This regional climate change was, however, derived from a coupled experiment without flux adjustment and, therefore, with significant biases in the simulated present-day SSTs.

The objective here is to assess the robustness of the Coupled Climate Model (CCM) monsoon response, not only to the global SST biases, but mainly to regional uncertainties in the projected global warming. Atmospheric time-slice experiments driven by prescribed SSTs are performed to explore the influence of present-day SSTs and of regional SST anomalies on the climate change simulated over South Asia. The focus is on two regional processes that have been identified in former global coupled scenarios as participating in the modulation of the simulated global warming, namely, the sea ice response at high latitudes and the El Niño–like response in the tropical Pacific Ocean (Meehl et al. 2000). The SST anomalies simulated in the southern high latitudes are very uncertain in the CCM, which is not able to simulate a realistic Antarctic sea ice cover during the

twentieth century (Douville et al. 2002). The SST anomalies are also highly model dependent in the tropical Pacific, where only a subset of coupled AOGCMs predict an El Niño–like response (Houghton et al. 2001). It is therefore particularly important to test the impact of such regional SST anomalies on the simulated Indian climate to assess the robustness of the monsoon response to global warming.

Section 2 describes the model and experiments. Section 3 briefly validates the simulated control climate and shows that, while the Indian monsoon response to increasing amounts of GHG is not very sensitive to the global SST biases of the CCM, it is influenced by the magnitude and pattern of SST anomalies prescribed in the Southern Ocean and in the tropical Pacific. Section 4 provides a brief discussion of the results and section 5 summarizes the main conclusions.

2. Model and experiments

a. The CNRM climate model

The CCM or the Centre National de Recherches Météorologiques (CNRM) CNRM-CM2 model has been described by Douville et al. (2002) and Ashrit et al. (2003). It is a coupled global climate model without flux adjustment, consisting of the ARPEGE AGCM (Déqué et al. 1994), the OPA OGCM (Madec et al. 1997), the Global Experimental Leads and Sea Ice for Atmosphere and Ocean (GELATO) sea ice model (Salas Méliá 2002), and the Interaction Sol–Biosphère–Atmosphère (ISBA) land surface model (Douville et al. 1995; Noilhan and Mahfouf 1996). The ARPEGE global atmospheric model is a spectral model with a progressive hybrid sigma pressure vertical coordinate, and here is used with a T63 truncation and 45 levels distributed between the earth’s surface and the upper stratosphere. The physical package includes the turbulence scheme of Louis et al. (1982), the statistical cloud scheme of Ricard and Royer (1993), and the mass flux convective scheme with Kuo-type closure of Bougeault (1985). The shortwave and longwave radiative schemes are derived from Morcrette (1989, 1990) and are activated every 3 h. The global ocean model used in this study has been developed at the Laboratoire d’Océanographie Dynamique et de Climatologie. It is a finite-difference model based on the primitive equations (Madec et al. 1997). It has 31 vertical levels with a much higher resolution in the boundary layer (10 m) than in the deep ocean (500 m). The horizontal grid has a variable resolution but a typical 2° interval in longitude while the latitude interval is about 0.5° at the equator and increases poleward. Sea ice is parameter-

ized with the GELATO dynamic and thermodynamic sea ice model, which considers several ice categories and an elastic-visco-plastic ice rheology (Salas Mélia 2002).

b. The reference climate scenario

In Ashrit et al. (2003), the CCM was used to produce two global climate scenarios, SG0 and SG1, spanning 150 yr. The simulations were initialized with oceanic temperature and salinity profiles from Levitus (1982) and with atmospheric trace gas concentrations observed in the 1950s and started with a 20-yr spinup period. After this spinup (and despite a residual drift in the Northern Hemisphere high latitudes due to a slow retreat of the Arctic sea ice), the GHG concentrations were updated each year according to observations from 1950 to 2000, and according to the Intergovernmental Panel on Climate Change (IPCC) Special Report on Emissions Scenarios (SRES) B2 marker scenario afterward. The global distribution of the sulfate aerosols was updated every 10 yr and specified according to the results of a transport model provided by Penner et al. (1998). Both direct and indirect effects of the aerosols were taken into account in the radiation parameterization according to Boucher and Lohman (1995). More details about the experiments can be found in Royer et al. (2002) and Douville et al. (2002).

In the present study, one of these two scenarios (SG1) is considered as a reference climate change experiment. Note that there is no particular reason for choosing SG1 instead of SG0. Both scenarios show very similar climate anomalies when comparing the last 50 yr (2050–99, hereafter referred to as P3) with the first 50 yr (1950–99, hereafter referred to as P1) of the integrations (Ashrit et al. 2003). As far as the present-day climate is concerned, the model biases are also very robust. Looking at the Indian summer monsoon season [June–September (JJAS)], the CCM shows a reasonable global distribution of SST (Fig. 1), but overestimated temperatures in the eastern part of the Atlantic and Pacific tropical oceans compared to the National Centers for Environmental Prediction–National Center for Atmospheric Research (NCEP–NCAR) climatology (available online at <http://dss.ucar.edu/datasets/ds090.0/data>). Such errors are found in many coupled AOGCMs and are probably due to a lack of marine stratus in the subtropical anticyclones. Large positive biases also appear in the circumpolar Southern Ocean, where the sea ice cover is strongly underestimated, and, to lesser extent, in the northern Pacific and northern Atlantic, where the simulation of sea ice is much more realistic.

Figure 2a shows the JJAS SST anomalies produced

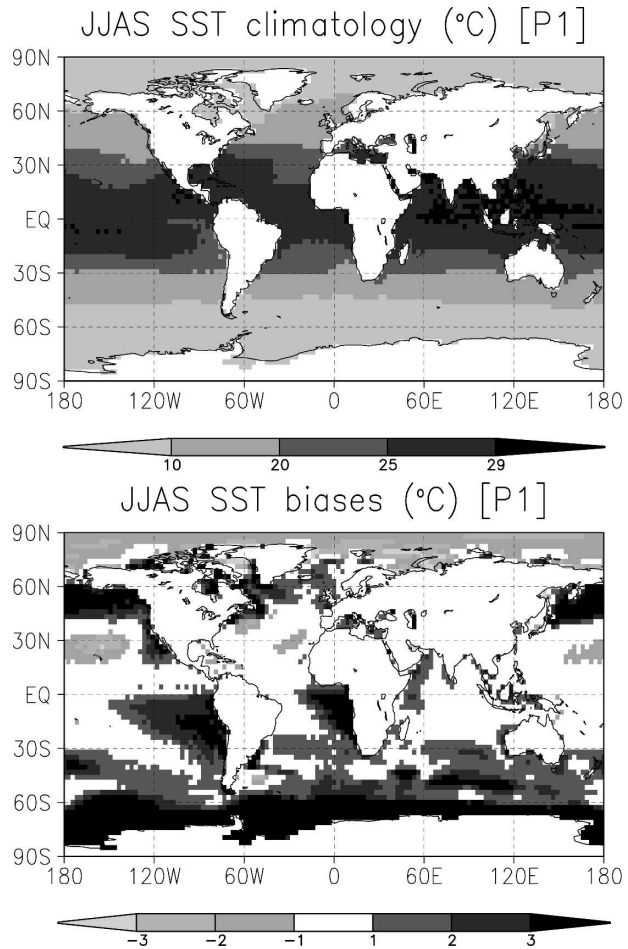


FIG. 1. Global JJAS distribution of (top) SST and of (bottom) SST biases relative to the NCEP–NCAR climatology in the coupled scenario SG1 during P1. All isolines are in $^{\circ}\text{C}$.

by the CCM when comparing the late twenty-first century (P3) with the late twentieth century (P1). Like in most IPCC scenarios, the maximum SST anomalies appear in the northern high latitudes, which can be partly explained by the retreat of the Arctic sea ice and of the Northern Hemisphere snow cover. In the southern high latitudes, the ocean warming is on the contrary very limited, which is due to the weaker extent of the land areas than in the Northern Hemisphere, and mostly to the lack of sea ice around the Antarctic from the beginning of the scenario. If sea ice is strongly underestimated during the twentieth century, the model cannot simulate the sea ice retreat during the twenty-first century and the southern high-latitude SST anomalies are probably underestimated (even if no significant warming was detected over the late twentieth century in the existing instrumental record over this region). In the tropical belt, the sea surface warming simulated by the

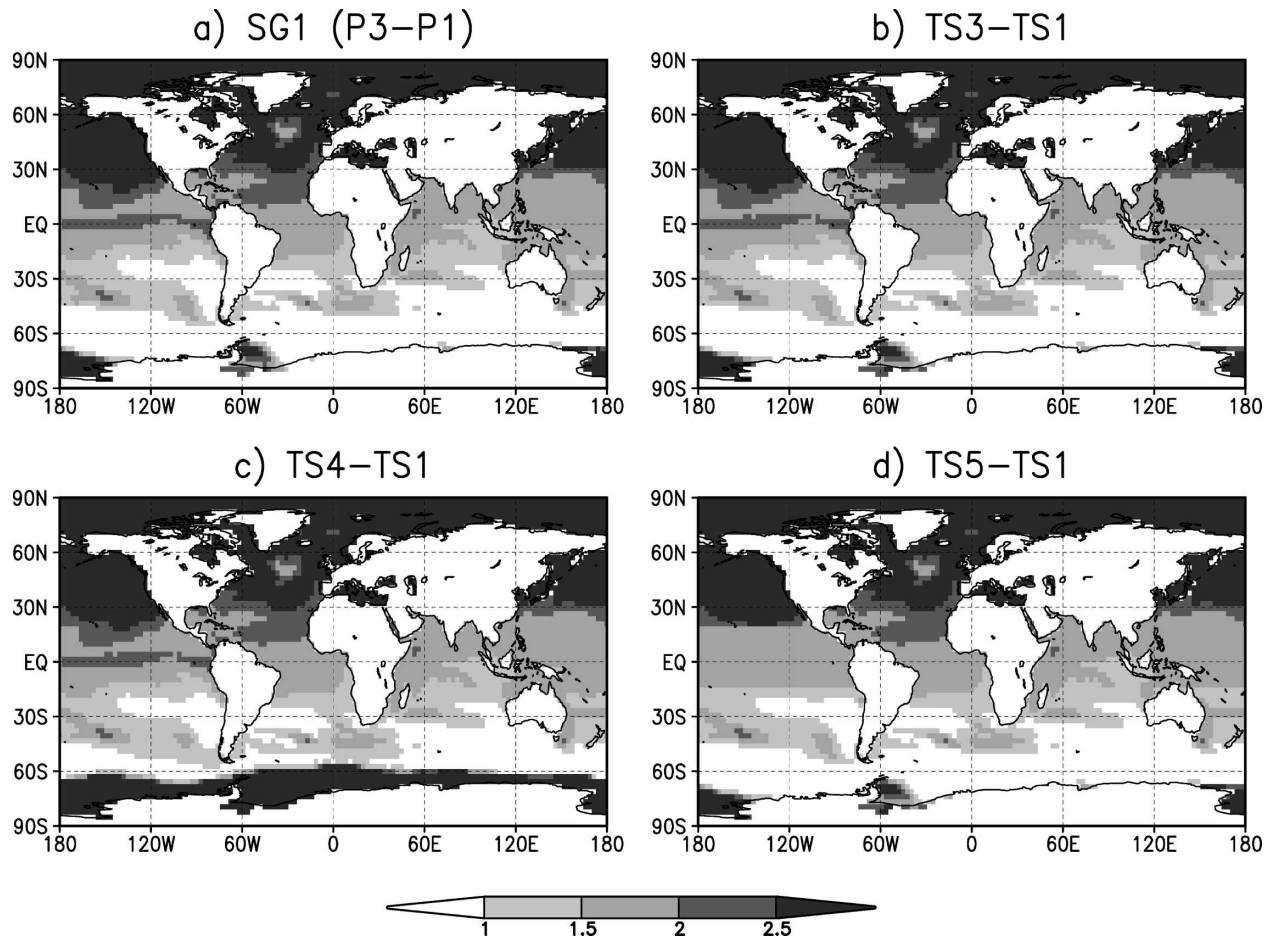


FIG. 2. Global JJAS distribution of simulated or prescribed SST anomalies in (a) SG1 (P3 – P1), (b) TS3 – TS1, (c) TS4 – TS1, and (d) TS5 – TS1. All isolines are in $^{\circ}\text{C}$.

CCM is generally between 1° and 2°C , except in the central and eastern equatorial Pacific where a tongue of SST anomalies exceeding 2°C clearly appears in Fig. 2a. Such an El Niño-like response is not specific to the CCM. It is, however, not systematic and might depend on the simulated cloud response (Meehl et al. 2000), and also on the present-day SST climatology in the equatorial Pacific. Given the significant SST biases of the CCM in the equatorial Pacific and in the southern high latitudes, it is important to investigate whether a different SST response in these regions would lead to a different monsoon response to global warming.

c. The time-slice experiments

The atmospheric response to increasing amounts of GHG can be thought of as partly due to a direct radiative effect and partly due to an indirect effect through changes in SST and sea ice boundary conditions. Several studies based on time-slice experiments (Stephen-

son and Held 1993; Déqué et al. 1998) have shown that the indirect effect is a dominant one, so that the main issue in designing such experiments is to decide how to prescribe the lower boundary conditions. In the present study, surface temperature has been prescribed not only over the open ocean but also over sea ice, which allows us to impose exactly the same surface ocean warming as in the reference scenario even in the high latitudes.

Three sets of time-slice experiments have been performed (Table 1) that share the same control simulation for present-day climate, but use different SST boundary conditions for simulating future climate. In the present-day climate integration (TS1), we prescribe climatological monthly mean SSTs derived from the NCEP–NCAR reanalyses to get rid of the CCM SST biases. In all future climate integrations (TS3, TS4, TS5), we prescribe SST boundary conditions that are based on the superimposition of the CCM monthly mean anomalies onto the NCEP–NCAR climatology.

TABLE 1. A summary of the experiments.

Expt	Prescribed concentrations of GHG and sulfate aerosols	SST boundary conditions	Duration (yr)
SG1	Year-by-year values from 1950 to 2099 (transient climate)	Coupled OGCM (reference coupled climate scenario)	150
TS1	1975 values (present-day climate)	NCEP–NCAR 1950–99 monthly mean climatology	10
TS3	2075 values (future climate)	NCEP–NCAR climatology + SG1 monthly mean climatological anomalies (P3–P1)	10
TS4	2075 values (future climate)	Same as in TS3, but with SG1–P3 monthly mean climatological SSTs around Antarctica	10
TS5	2075 values (future climate)	Same as in TS3, but with zonally averaged monthly mean climatological anomalies (P3–P1) in the tropical Pacific	10

In TS3, the prescribed SST anomalies are exactly the same as in SG1 (Fig. 2b). In TS4, SSTs prescribed around the Antarctic are directly derived from SG1 (raw SST climatology during P3) so that the prescribed surface warming is much stronger than in SG1 (Fig. 2c). A bilinear interpolation is used around 60°S to ensure a smooth transition between the midlatitudes and the high latitudes. In TS5, the El Niño–like response in the tropical Pacific is removed by prescribing zonal mean SST anomalies between 20°S and 20°N in this ocean basin (Fig. 2d).

All simulations are 10-yr atmospheric integrations without interannual variability in the SST boundary conditions. Such an experiment design was justified by Douville (2005) who demonstrated that interannual SST fluctuations could lead to spurious impacts on the simulated tropical atmospheric response in such time-slice experiments without ocean feedbacks. This conclusion was recently reinforced by Krishna Kumar et al. (2005) who showed that prescribing observed SSTs in the warm pool regions of the Indo-West Pacific Ocean could lead to a decrease in the actual seasonal predictability of the Indian summer monsoon compared with the use of coupled or climatological SSTs outside the eastern tropical Pacific.

In addition to lower boundary conditions, concentrations of GHG and sulfate aerosols must be also prescribed. For the sake of simplicity, the concentrations prescribed in TS1 have been fixed at the level found in the middle of P1 (1975) in SG1. Similarly, the future climate integrations have been forced by concentrations derived from 2075 (middle of P3).

3. Results

a. Brief validation of the present-day monsoon climate

Before comparing the response of the Indian summer monsoon in the various sets of time-slice experiments,

the simulation of the present-day monsoon climate is here briefly validated against the NCEP–NCAR atmospheric reanalyses and the Climatic Research Unit (CRU; available online at <http://www.cru.uea.ac.uk/cru/data>) or the Global Precipitation Climatology Project (GPCP; Huffman et al. 1997) precipitation climatology. More details about the validation of the CCM can be found in Douville et al. (2002), Salas Méliá (2002), and Ashrit et al. (2003).

Looking first at the mean annual cycle, Fig. 3a focuses on the dynamical Indian monsoon index (IMI) proposed by Wang et al. (2001). This index reflects both the intensity of the monsoon flow over the Arabian Sea and of the low-level vorticity anomalies associated with north Indian low pressures. Both SG1 and TS1 show a realistic reversal of the IMI between May and October. Also well captured is the strong annual cycle of precipitation over the Indian subcontinent (Fig. 3b). Comparing TS1 with SG1 does not reveal any dramatic impact of using observed rather than interactive SSTs. The main difference is a relative weakening and an earlier beginning of the summer monsoon, which does not improve the model climatology.

Figure 4 shows the spatial distribution of the low-level zonal wind averaged over JJAS. Both SG1 and TS1 underestimated the westerly monsoon flow over the northern Indian Ocean and South Asia and the easterlies over the central equatorial Pacific. TS1 shows additional biases in the eastern Indian Ocean and western Pacific. As far as precipitation is concerned, SG1 overestimated JJAS accumulation over the Arabian Sea and underestimated monsoon rainfall over Bangladesh (Fig. 5). Nevertheless, the model is able to simulate some regional features of the Indian monsoon rainfall, such as the east–west contrast, and shows a reasonable climatology compared to many other AGCMs (Gadgil and Sajani 1998). Similar to low-level winds, precipitation is not necessarily better simulated in

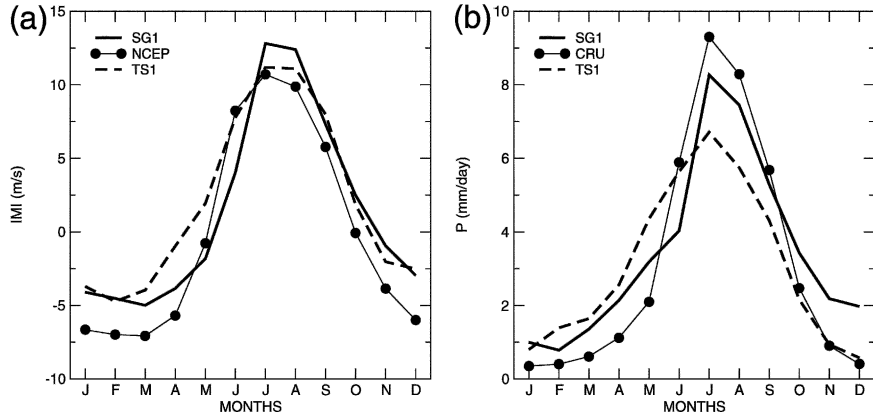


FIG. 3. Observed and simulated annual cycle of the monthly monsoon indices averaged over P1: (a) dynamical IMI (see definition in section 3a), and (b) precipitation over land between 5°–30°N and 70°–95°E.

TS1. Prescribing observed SSTs does not improve the ARPEGE monsoon climatology. The ocean–atmosphere coupling is known to play a crucial role in the Tropics, both at intraseasonal [Madden–Julian oscillation

(MJO)] and interannual (ENSO) time scales. It could explain why a coupled model performs better than the same AGCM forced with observed SSTs in the Indo-Pacific domain.

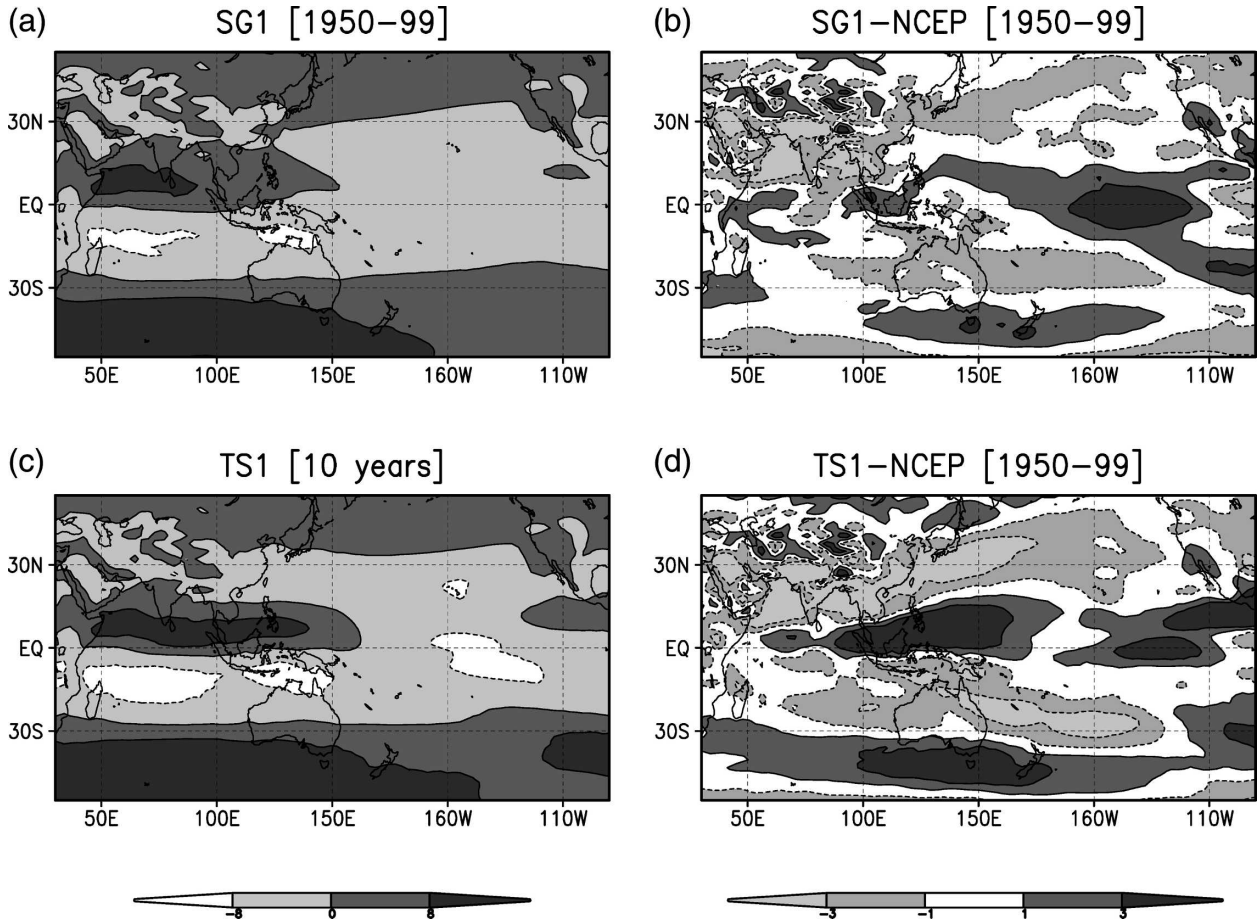


FIG. 4. Indo-Pacific summer (JJAS) distribution of 850-hPa zonal wind (m s^{-1}) for (a) SG1 during P1, (b) SG1 – NCEP–NCAR, (c) TS1, and (d) TS1 – NCEP–NCAR.

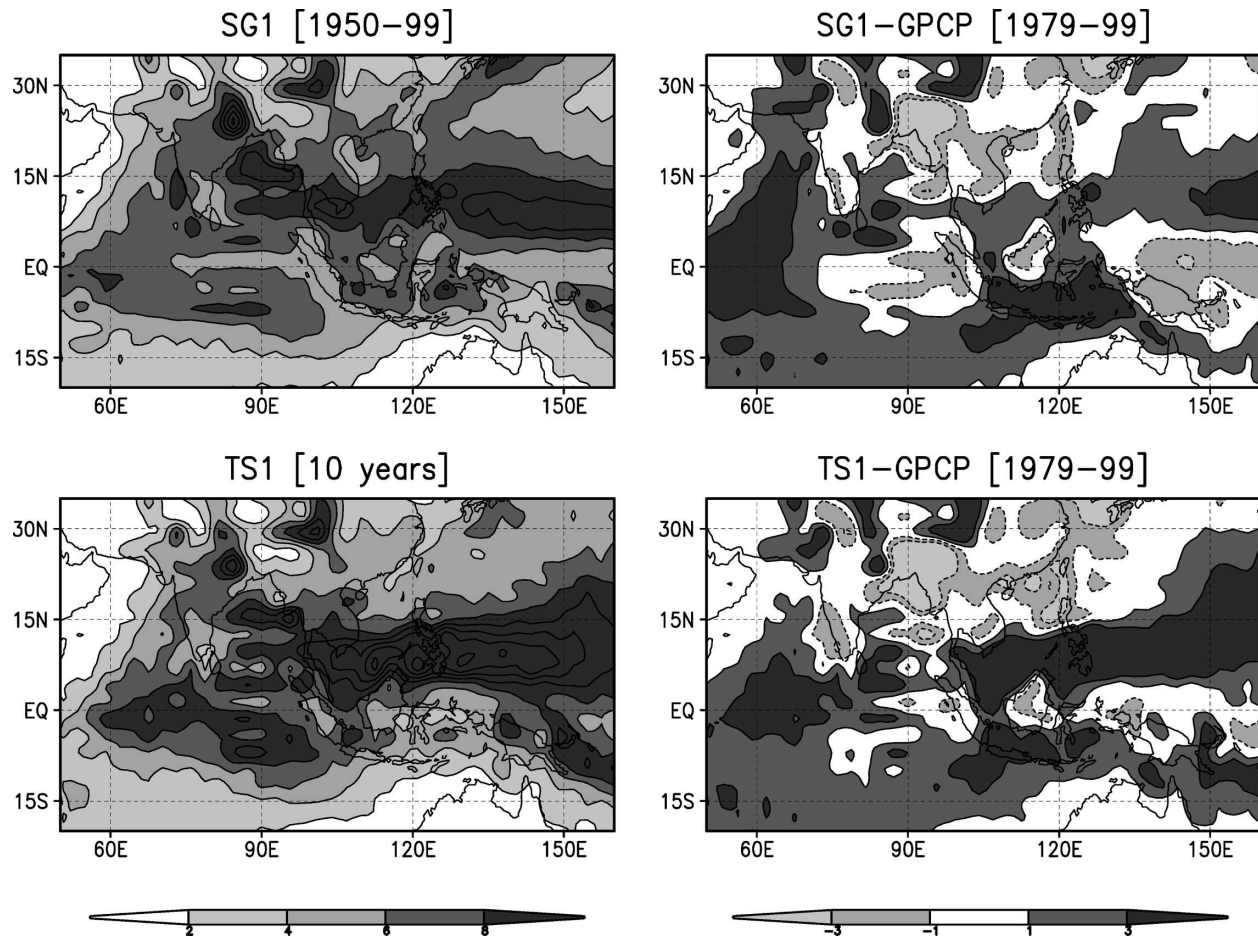


FIG. 5. Same as in Fig. 4, but for JJAS precipitation (mm day^{-1}) and with the GPCP observed climatology (1979–99).

b. Regional climate change

Figure 6 compares the mean annual cycle of regional climate anomalies in the transient scenario and in the various time-slice experiments. Looking first at the monsoon response in SG1 (solid red line), Fig. 6a shows a weakening of the IMI from June to September. Despite this weaker low-level circulation, the all-India precipitation is increased during the monsoon season (Fig. 6b). This apparent paradox has been discussed in detail by Ashrit et al. (2003), and in former studies (Kitoh et al. 1997; Douville et al. 2000b). The main explanation is related to an increase in precipitable water in a warmer climate, so that moisture convergence can be reinforced without increase in mass convergence.

When the prescribed SST anomalies are exactly the same as in SG1 ($\text{TS3} - \text{TS1}$), the time-slice experiments do not predict exactly the same monsoon response as in the transient scenario, at least at the monthly time scale. Such a mismatch between the predicted climate change in the forced versus coupled experiments occurs

for at least three reasons (Douville 2005). First, the approximate radiative forcing used in the time-slice experiments has a limited, but significant, impact on the land surface temperature and thereby on the monsoon sensitivity to global warming. Second, the lack of interannual SST variability also alters the monsoon response since the detailed regional distribution of the JJAS precipitation anomalies simulated by the CCM within the Tropics is sensitive to the ENSO variability. Last, the lack of SST feedback also affects the SST–convection relationship, which in turn can affect the mean Walker and/or Hadley circulation and thereby the monsoon and its response to global warming.

However, $\text{TS1}/\text{TS3}$ roughly reproduce the increase in monsoon rainfall found in the transient scenario. The main objective of the present study is therefore to assess the sensitivity of this precipitation response to the regional SST anomalies prescribed in TS4 and TS5 . Figure 6 suggests that this sensitivity is not negligible, especially for zonal mean instead of El Niño-like SST anomalies in the tropical Pacific. In TS5 , the July and

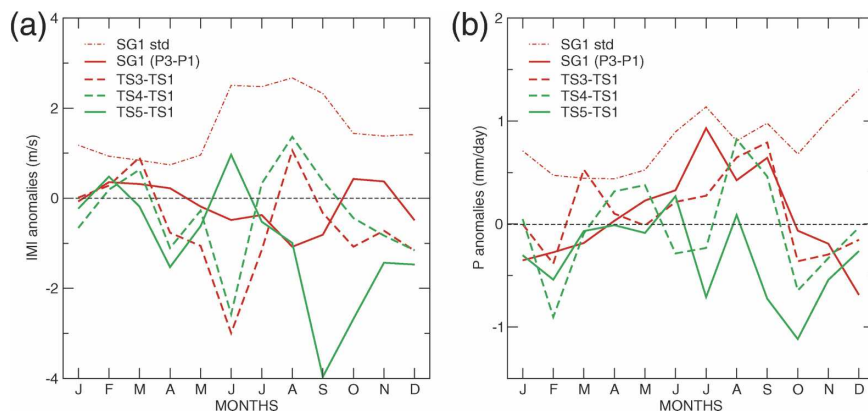


FIG. 6. Annual cycle of anomalies ($P3 - P1$) in monthly monsoon indices: (a) dynamical IMI, and (b) precipitation over land between 5° – 30° N and 70° – 95° E. Also shown are the monthly standard deviations estimated over $P1$ in SG1 (thin dotted-dashed red line).

late monsoon precipitation indeed show a strong decrease that is not found in TS3 and in the coupled scenario. TS4 is more similar to TS3, but shows decreased rather than increased precipitation in June–July.

Moving to the spatial distribution of the JJAS climate change, Fig. 7 shows the low-level zonal wind anomalies ($P3 - P1$) simulated in SG1, the corresponding anomalies in the first set of time-slice experiments (TS3 –

TS1), and the differences between the monsoon response found in TS1/TS3 and the other time-slice experiments. The t test is systematically applied to assess the statistical significance of the results. As discussed by Ashrit et al. (2003), SG1 shows a weakening and a northward shift of the monsoon flow with enhanced concentrations of GHG (Fig. 7a). The winter westerlies are reinforced in the southern midlatitudes. A weaken-

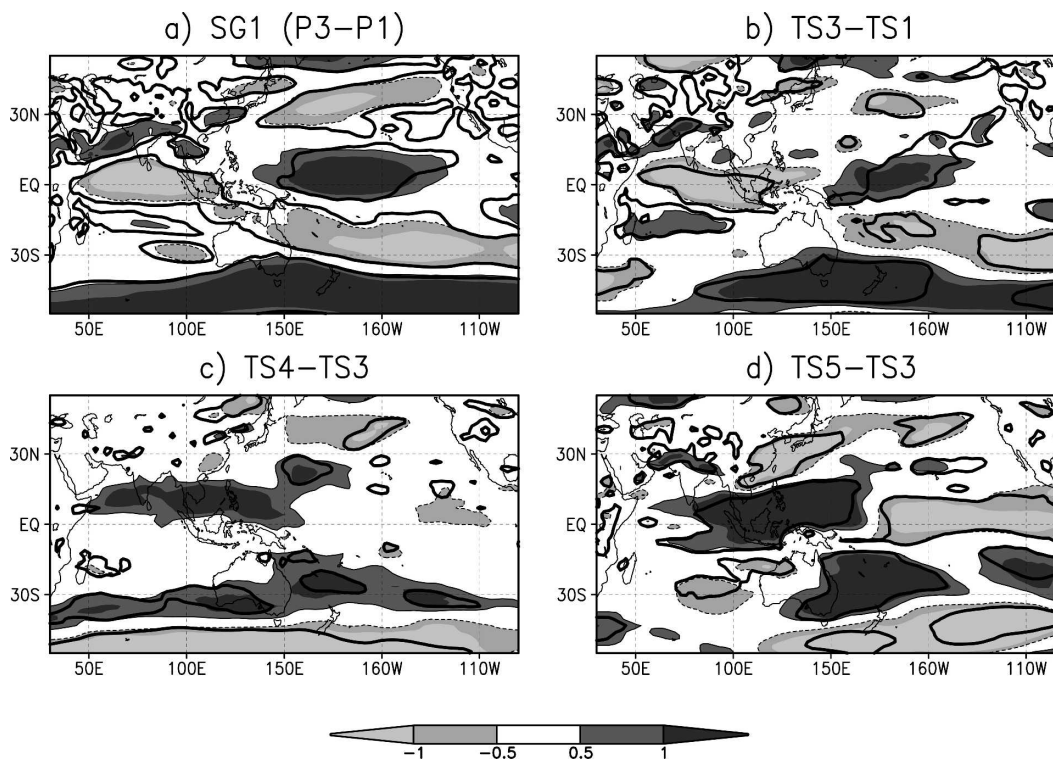


FIG. 7. Indo-Pacific summer (JJAS) distribution of 850-hPa zonal wind anomalies (m s^{-1}) for (a) $P3 - P1$ in SG1 (coupled response), (b) $TS3 - TS1$, (c) $TS4 - TS3$, and (d) $TS5 - TS3$. Thick black solid lines indicate differences that are significant at the 5% level.

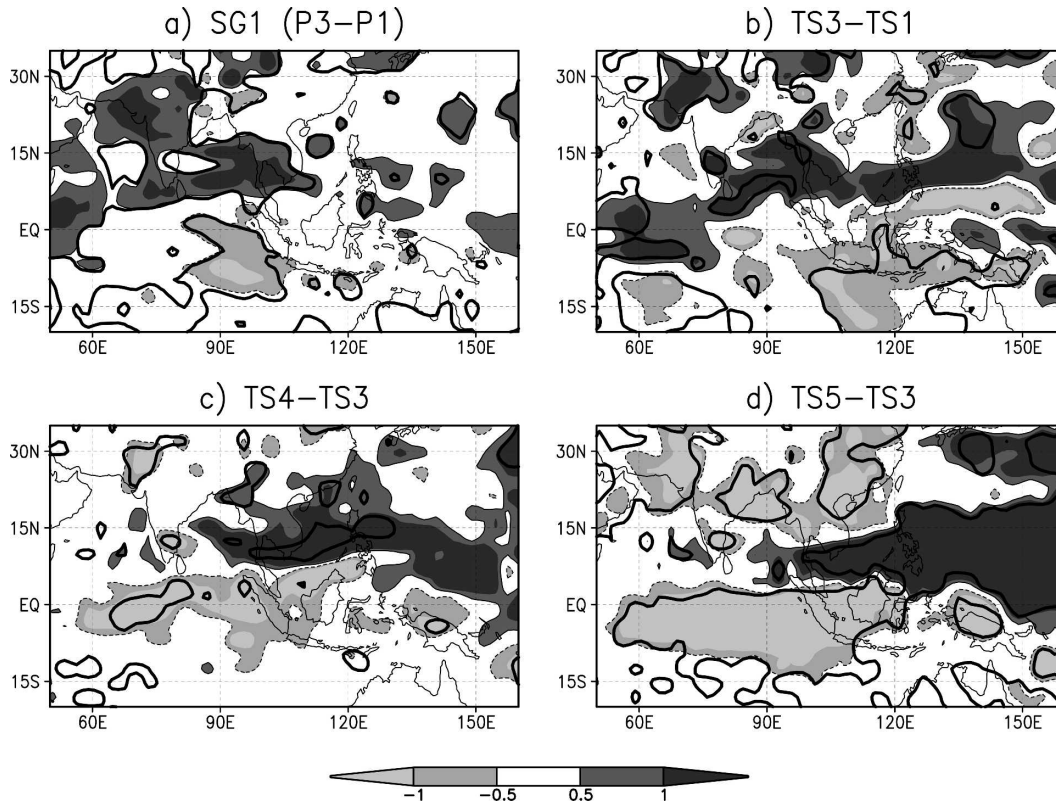


FIG. 8. Same as in Fig. 7, but for JJAS precipitation anomalies (mm day^{-1}).

ing of the equatorial easterlies is found in the central Pacific, which is surrounded by easterly zonal wind anomalies in the subtropics. This large-scale response is fairly well reproduced by TS1/TS3 (Fig. 7b). In TS4, prescribing larger SST anomalies in the circumpolar Southern Ocean leads to a northward shift of the meridional temperature gradient, and therefore of the westerlies in the southern midlatitudes. Remote impacts are also found in the Tropics, with a strengthening of the monsoon flow that is, however, not significant at the 5% level (Fig. 7c). In TS5, prescribing zonal mean SST anomalies in the tropical Pacific has a stronger impact on the low-level wind response to global warming (Fig. 7d). In the intertropical convergence zone, there are westward anomalies over the eastern Indian Ocean and western Pacific, and eastward anomalies over the eastern Pacific, leading to a stronger low-level convergence in the central Pacific. Also noticeable are a strengthening of the monsoon flow over northern India and a northward shift of the midlatitudes westerlies over the southern Pacific.

Moving to the JJAS precipitation change, Fig. 8a shows enhanced monsoon rainfall over a large fraction of the Indian subcontinent in SG1. The first set of time-slice experiments, TS1/TS3, is able to capture the main

features of the coupled precipitation response over South Asia, though it does not show a significant increase in monsoon rainfall over central India, but only over the northwest and the southern tip of the peninsula. Moreover, the precipitation response is clearly different from that found in SG1 in the tropical western Pacific. Note again that this relative mismatch between the forced and coupled projected climate change has been discussed in detail by Douville (2005). Our main objective here is to demonstrate that, while TS1/TS3 produce regional climate anomalies that are rather consistent with the coupled scenario, such anomalies are, however, not robust since even minor modifications in the prescribed SST forcing are likely to induce significant atmospheric anomalies over South Asia. This is obvious in Fig. 8d, where the impact of global warming on the Indian monsoon rainfall is partly offset by the zonal averaging of the tropical Pacific SST anomalies. Such a modification in the SST forcing also has a strong impact on the simulated precipitation in the western Pacific and southern Indian Ocean. Prescribing a stronger warming in the southern high latitudes has a weaker impact on the precipitation response (Fig. 8c), especially over India where the precipitation increase is however weaker than in TS1/TS3.

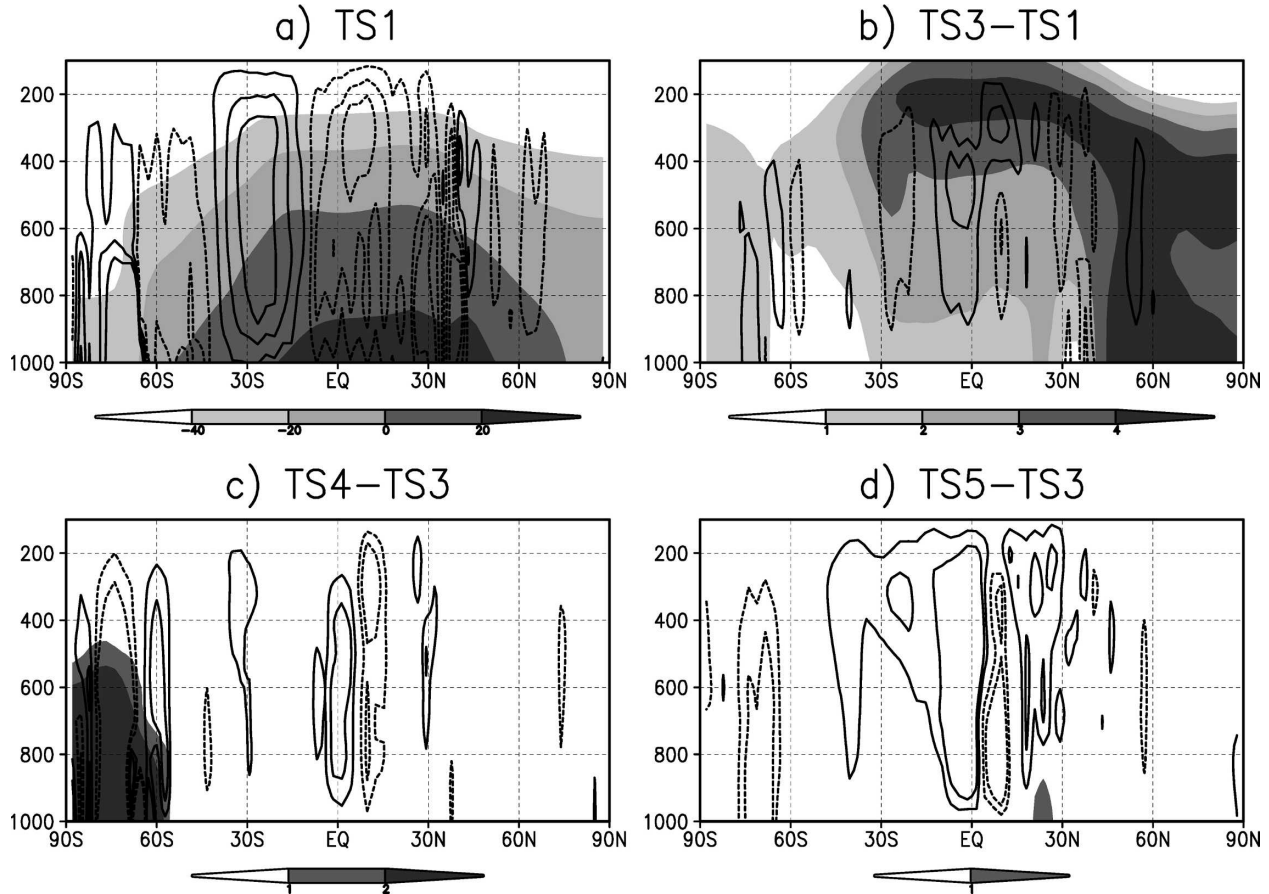


FIG. 9. Latitude–pressure cross section of JJAS temperature ($^{\circ}\text{C}$) and vertical velocity (Pa s^{-1}) averaged between 70° and 110°E for (a) TS1, (b) TS3 – TS1, (c) TS4 – TS3, and (d) TS5 – TS3. Vertical velocity isolines are every 0.02 Pa s^{-1} for control values and -0.01 , -0.005 , 0.005 , and 0.01 Pa s^{-1} , respectively, for anomalies; negative contours are dashed and indicate upward velocity.

c. Changes in Hadley and Walker circulations

The Asian monsoon plays an active role in the global atmospheric circulation, particularly through its interaction with the Hadley and Walker circulations. It is therefore useful to look at vertical cross sections in the troposphere to better understand the monsoon response in our sensitivity experiments.

Figure 9 first shows the latitude–pressure cross section of temperature and vertical velocity (dp/dt) averaged between 70° and 110°E . In TS1 (Fig. 9a), vertical velocity shows strong negative values between 0° and 35°N , indicating upward motion over India and the equatorial Indian Ocean. The descending branch of the regional Hadley cell appears clearly around 30°S with a maximum of positive vertical velocity. In Fig. 9b, the enhanced greenhouse effect (TS3 – TS1) produces a strong warming in the Northern Hemisphere low troposphere and in the tropical upper troposphere. Changes in vertical velocity indicate increased convection over northern India, but decreased convection

over the equatorial Indian Ocean, in keeping with the precipitation response found in Fig. 8b. Looking at the impact of the regional SST anomalies superimposed onto the prescribed global warming, as expected TS4 – TS3 (Fig. 9c) shows a low-level warming in the southern high latitudes and some perturbations in the distribution of vertical motion. A local weakening of the so-called Ferrel cell appears in the southern high latitudes. Remote impacts are also found in the Tropics that are consistent with the precipitation anomalies presented in Fig. 8c. Changes in vertical velocity that somewhat resemble the impacts found in TS4, though the prescribed SST anomalies are now located in the tropical Pacific, are shown in TS5 – TS3 (Fig. 9d).

Figure 10 provides a better perspective on the regional Hadley circulation by showing the latitude–pressure cross section of meridional wind and vertical velocity averaged between 70° and 110°E . Figure 10a shows the results of TS1 and confirms that upward motion in the midtroposphere is associated with low-level

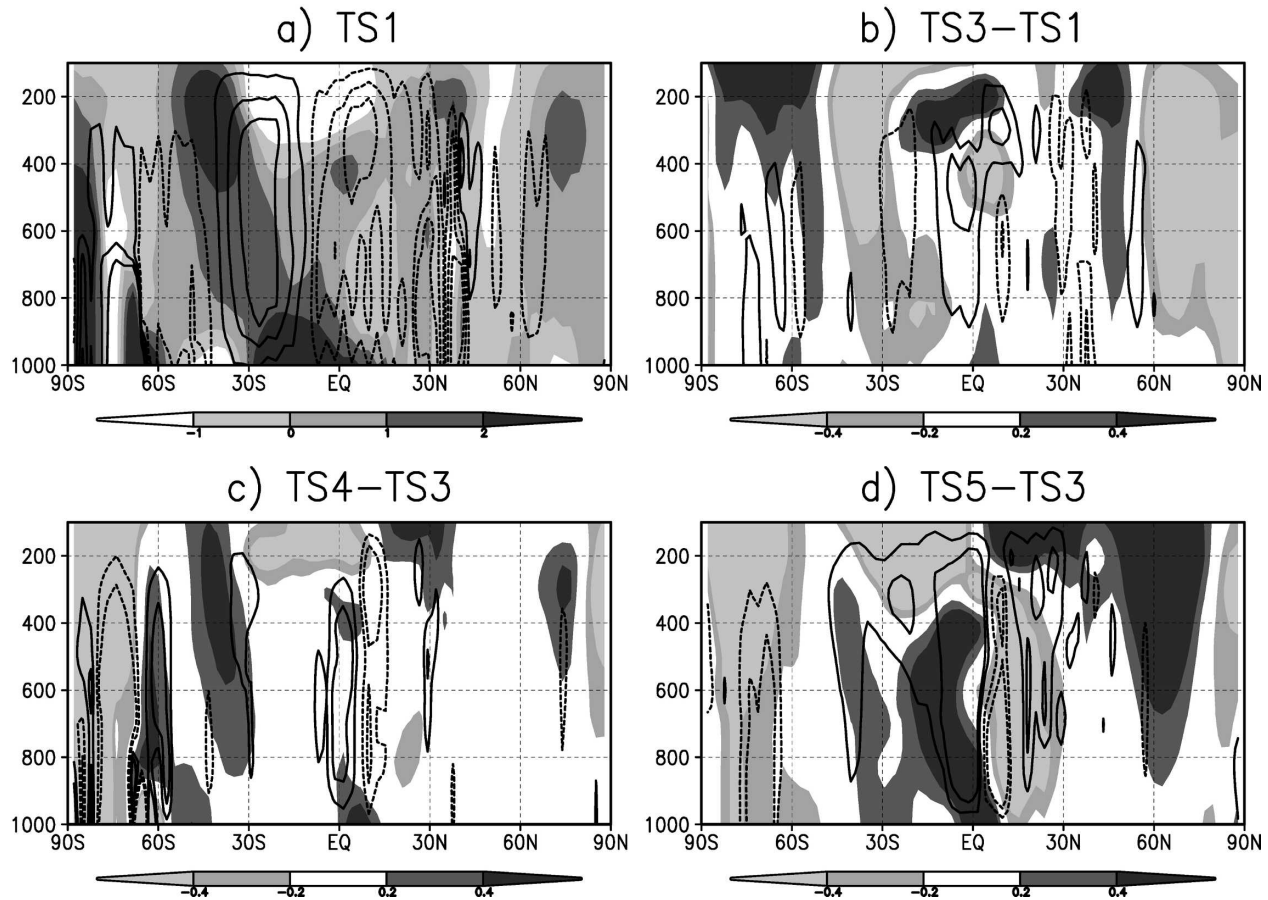


FIG. 10. Same as in Fig. 9, but for JJAS meridional wind (m s^{-1}) and vertical velocity (Pa s^{-1}).

convergence and upper-level divergence. The impact of global warming (TS3 – TS1, Fig. 10b) shows a weakening and a northward shift of the regional Hadley circulation, in keeping with the coupled model response (Ashrit et al. 2003). TS4 – TS3 anomalies (Fig. 10c) suggest a northward shift and a strengthening of the regional Hadley circulation, but the link with the southern high-latitude warming is not obvious and will be further discussed in section 4. TS5 – TS3 shows a stronger perturbation of the tropical circulation, with an increased low-level convergence north of the equator, associated with a cyclonic anomaly over the Pacific warm pool and with enhanced Mascarene high pressures in the southern Indian Ocean (not shown). The impact is also pronounced at 200 hPa, where an interhemispheric dipole of meridional wind anomalies, associated with a limited anomaly of vertical velocity north of the equator, suggests that the upper-level divergent anomaly is an indirect response to changes in the Walker circulation rather than a direct response of the regional Hadley circulation.

Figure 11 shows the longitude–pressure cross section

of zonal wind and vertical velocity averaged between 5°S and 5°N . Figure 11a first illustrates the present-day Walker circulation simulated by TS1, with the descending branch over the eastern Pacific and ascending branch over the western Pacific and the Indian Ocean. TS3 – TS1 (Fig. 11b) shows a weakening of both the north equatorial monsoon flow and the west Pacific easterlies. The global warming therefore leads to a weakening of the Walker circulation over the equatorial Pacific, in keeping with the coupled model response described by Ashrit et al. (2003). Removing the El Niño–like pattern in the tropical Pacific SST anomalies (TS5 – TS3, Fig. 11d) does not lead to the full recovery of the present-day Walker circulation, but rather to a regional perturbation whereby enhanced convection over the western Pacific induces downward velocity anomalies over the Indian Ocean, as if there was a competition of convection between the two regions. Such a result confirms that the downward anomalies of vertical velocity found above the Indian Ocean (Fig. 10d) are the consequence of a perturbation in the Walker circulation. TS4 – TS3 (Fig. 11c) shows

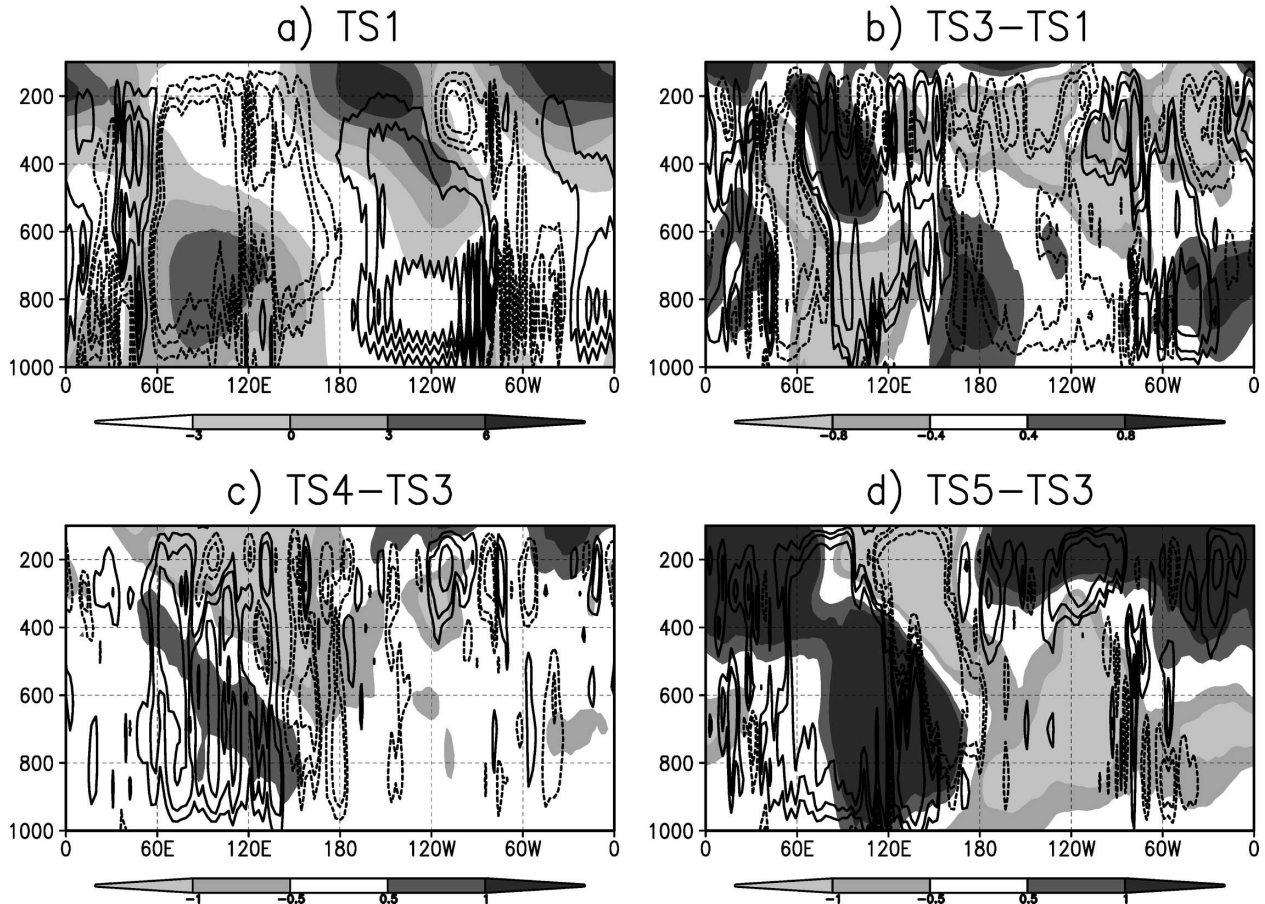


FIG. 11. Longitude–pressure cross section of JJAS zonal wind (m s^{-1}) and vertical velocity (Pa s^{-1}) averaged between 5°S and 5°N : (a) TS1, (b) TS3 – TS1, (c) TS4 – TS3, and (d) TS5 – TS3. Vertical velocity isolines are every 0.02 Pa s^{-1} for control values and are -0.01 , -0.005 , 0.005 , and 0.01 Pa s^{-1} , respectively, for anomalies; negative contours are dashed and indicate upward velocity.

a weaker and less homogeneous response that is, however, somewhat similar to the impact found in TS5. Such a similarity, already apparent in Figs. 9 and 10, highlights the strong interaction between the Hadley and Walker circulations in our AGCM.

Finally, Fig. 12 shows the longitude–pressure cross section of specific humidity and vertical velocity averaged between 5°S and 5°N . While global warming (Fig. 12b) leads to a general increase in tropospheric water content, experiments with regional SST anomalies show enhanced (reduced) specific humidity in areas of upward (downward) anomalies of vertical velocity, thereby indicating that deep convection plays a crucial role in maintaining dynamical anomalies via the release of latent heat in the middle and upper troposphere. The dipole anomaly of specific humidity in Fig. 12d provides another explanation for the decreased monsoon precipitation over India in TS5 compared to TS3. A fraction of the water vapor transported by the Pacific easterlies is trapped by the low-level convergence anomaly

associated with the enhanced convection in the west Pacific, and thereby does not feed the monsoon flow and the Indian monsoon precipitation.

4. Discussion

In the present study, sensitivity experiments to uncertainties in the surface oceanic warming caused by increasing amounts of GHG have been performed for two key regions where the projected twenty-first century SST anomalies are strongly model dependent (Meehl et al. 2000; Houghton et al. 2001; Yu and Boer 2002).

a. Tropical Pacific

The first region is the tropical Pacific, where the CCM shows an El Niño-like response to enhanced greenhouse effect, characterized by greater surface warming in the eastern tropical Pacific compared to the

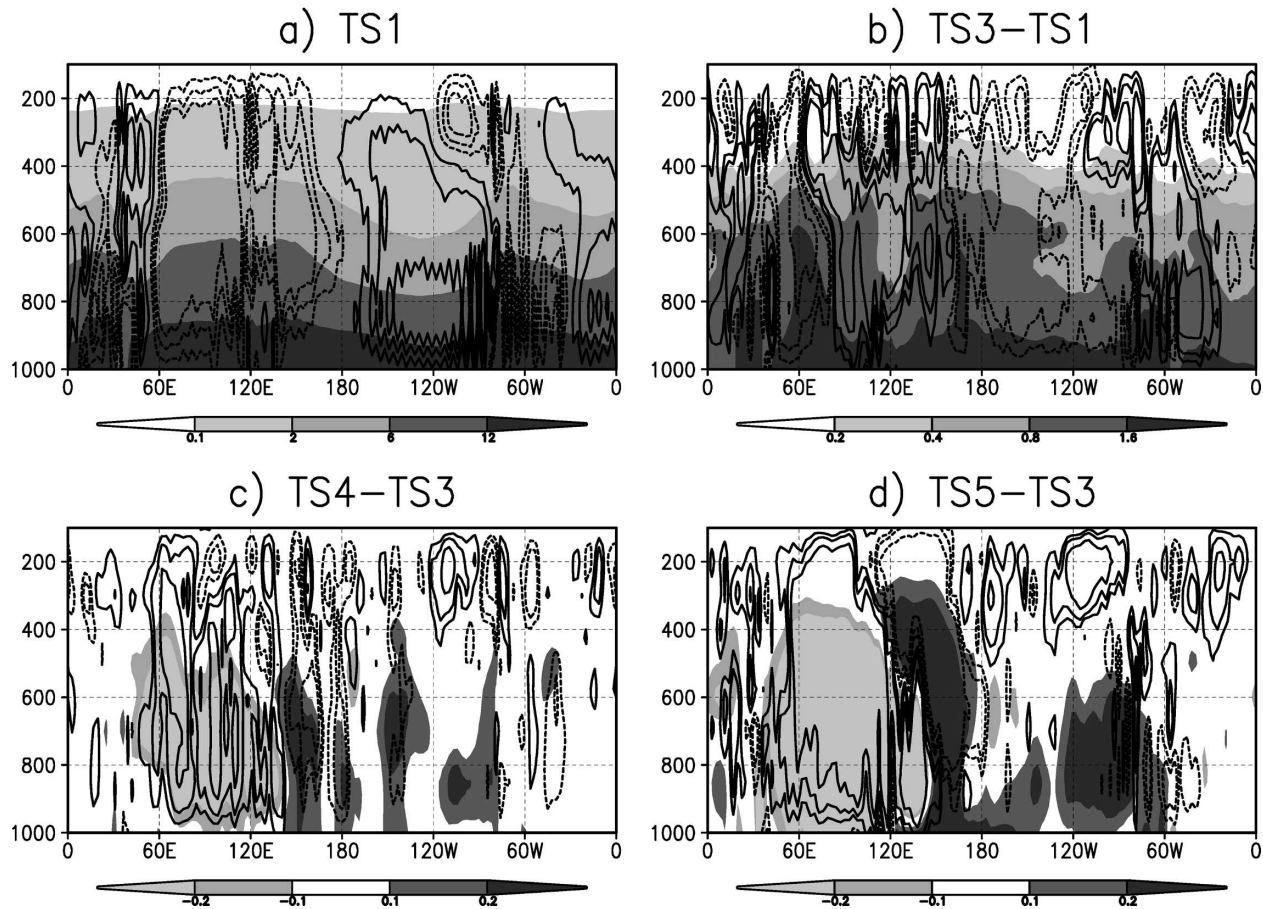


FIG. 12. Same as in Fig. 11, but for JJAS specific humidity (g kg^{-1}) and vertical velocity (Pa s^{-1}).

western Pacific. It is important to note the climatological nature of this pattern, which must be distinguished from the interannual ENSO signal. The existence of a mean El Niño-like pattern does not imply that the system locks onto the warm phase of ENSO, but rather that it shows a reduced asymmetry in the equatorial Pacific SST. The El Niño-like response of the CCM is robust and was found not only in SG1, but also in three other SRES-B2 coupled scenarios conducted with slightly different versions of the ARPEGE atmospheric model (not shown). It is a relatively common feature since a majority of coupled models simulate a similar reduction of the zonal equatorial SST gradient in the Pacific over the twenty-first century (see Yu and Boer 2002 for a brief review). This is the case in particular for the ECHAM4/OPYC3 model (Timmermann et al. 1999) that, interestingly, shows the same ENSO characteristics as the CCM (i.e., a realistic amplitude of the SST variability in the tropical Pacific and realistic ENSO teleconnections, but a too short and too regular ENSO cycle; Camberlin et al. 2004). However, while the mean El Niño-like response in this model is asso-

ciated with an increased ENSO variability, the CCM does not predict any clear change in variability (Ashrit et al. 2003). Conversely, several climate change studies do not show El Niño-like Pacific SST anomalies. For example, Meehl et al. (2000) performed equilibrium sensitivity experiments to doubled CO_2 with two different AGCMs coupled to the same slab ocean model and found an El Niño-like response in only one of them, due to contrasted cloud responses in the eastern equatorial Pacific.

Given the diversity of the Pacific SST response to global warming in different models, it is important to explore the relevance of this uncertainty for the future climate simulated with a given model. Such a question has been here addressed by performing parallel time-slice experiments in which the tropical Pacific SST anomalies have been either directly prescribed from the CCM or zonally averaged. The atmospheric response is somewhat surprising since the impact on the Indian monsoon is not the one that is observed on the seasonal time scale. While La Niña events are generally associated with increased Indian summer monsoon rainfall,

the removal of the El Niño-like SST pattern in the prescribed climatological SST warming leads to decreased monsoon precipitation. Therefore, the teleconnections that are useful to understand the natural climate variability are not necessarily relevant for predicting the climate response to enhanced concentrations of GHG. Note, however, that the absence of tropical SST feedbacks is a serious limitation of the time-slice experiments (Kitoh and Arakawa 1999; Douville 2005), and that the atmospheric sensitivity to the Pacific SST anomalies might have been overestimated in the present study.

b. Southern Ocean

The second region that has been given particular attention is the circumpolar Southern Ocean, where the sea ice response is a major uncertainty in determining the surface warming. Many coupled models, which, like the CCM, do not use any flux adjustment, still show serious deficiencies in simulating sea ice. While it is generally assumed that the Antarctic sea ice should be less sensitive to global warming than the Arctic sea ice, the CCM provides a somewhat extreme scenario since the sea ice retreat is very limited because of the strong underestimation of the present-day sea ice extent. It has therefore been decided to perform a sensitivity time-slice experiment corresponding to a symmetric hypothesis (i.e., the removal of most of the Antarctic sea ice even during the austral winter season). Experiments TS3 and TS4 are therefore designed to study the sensitivity of the Indian monsoon response to extreme but opposite sea ice feedbacks in the Southern Ocean, while keeping the same SST anomalies in the other oceans.

Similar sensitivity tests to the Antarctic sea ice extent were conducted several years ago with other AGCMs forced by present-day SST climatologies. For example, Mitchell and Senior (1989) removed all Southern Hemisphere sea ice equatorward of 67.5°S in their AGCM and found a local decrease in surface pressure, and a dipole of zonal wind anomalies in the region of the extratropical westerly jet, as expected from the thermal wind relationship. More recently, Menendez et al. (1999) performed a similar sensitivity test and showed a significant impact throughout the troposphere. Both falls and rises in sea level pressure were found in the region from which the sea ice was removed. The winter westerlies were reduced and shifted equatorward, in keeping with the results of Mitchell and Senior (1989). This significant impact on the mean atmospheric circulation was associated with changes in the eddy activity, leading to a weakening of the pole-

ward transient temperature flux and of the eddy flux convergence of westerly momentum.

Though looking at future rather than present-day climate, TS4 – TS3 shows a similar atmospheric response in the southern extratropics. In particular, the weakening and equatorward shift of the Southern Hemisphere westerlies is very clear (not shown) and represents a strengthening of the zonal mean response to global warming. This effect is zonally symmetric and is therefore also found above the Indian Ocean. However, while this longitude domain shows a weakening of the tropical easterly jet in TS3 compared to TS1, this tropical impact is offset in TS4 by the stronger SST warming prescribed in the circumpolar Southern Ocean. Such a remote impact of the Southern Hemisphere sea ice extent in the Tropics was not found in Mitchell and Senior (1989) and Menendez et al. (1999) and is not easy to explain. Changes in the regional meridional circulation (Fig. 10c) indicate a strengthening and an equatorward shift of the regional Hadley circulation. The shift is consistent with the displacement of the meridional gradient of temperature and of the midlatitude westerlies. This strengthening could be related to the decrease in the temperature gradient between the Tropics and the southern high latitudes. Such a decrease should lead to a reduced cyclonic activity, and thereby to a stronger accumulation of momentum and energy in the Tropics. However, the mechanisms whereby a reduction in the poleward transport can reinforce the Hadley circulation remain unclear and cannot be understood without a detailed analysis at the synoptic time scale. However, note that observational studies confirm the possible relationship between Antarctic sea ice extent and tropical climate variability. For example, Yuan and Martinson (2000) found significant correlations of detrended Antarctic sea ice edge anomalies with the ENSO and with the tropical Indian Ocean SST. While such results are generally interpreted as the impact of tropical variability on the southern high latitudes, cross correlations also provide some evidence of sea ice conditions preceding tropical anomalies (Simmonds and Jacka 1995).

5. Summary

This study is the continuation of Ashrit et al. (2003) who analyzed the response of the Indian summer monsoon to increasing amounts of GHG (and varying concentrations of sulfate aerosols) in two transient coupled climate scenarios based on the CCM. The objective is to assess the robustness of the regional climate change simulated over India by performing additional atmospheric time-slice experiments with prescribed SSTs. The control atmospheric simulation (TS1) is forced by

the NCEP–NCAR monthly mean SST climatology, while the future climate integrations are forced by climatological monthly mean SSTs constructed as the sum of the NCEP–NCAR climatology and of the monthly mean SST anomalies derived from a reference climate scenario (climatological anomalies between the late twenty-first century and the late twentieth century of scenario SG1). In addition to a first future climate integration (TS3) with exactly the same sea surface warming as in SG1, two more experiments have been performed to test the sensitivity of the monsoon response to regional SST anomalies in the southern high latitudes (TS4) or the tropical Pacific (TS5). These are indeed two key regions of high uncertainty that are likely to modulate the global warming predicted by the CCM.

The results first indicate that the ARPEGE AGCM is able to reproduce, at least qualitatively, the Indian monsoon response found in the CCM, despite the use of prescribed observed rather than interactive SSTs. Therefore, the SST biases found in the CCM have a limited direct impact on the atmospheric response to increasing amounts of GHG (an indirect impact is, however, possible through their influence on the prescribed SST anomalies). Moreover, the lack of SST feedback and variability in the time-slice experiments does not seem to be a major obstacle for capturing the CCM monsoon projection. Such a conclusion must be however tempered by the results of Douville (2005) who demonstrated that time-slice experiments driven directly by the raw SSTs of SG1 could not accurately reproduce the monsoon response found in the CCM. In other words, the relative consistency between the monsoon response found in SG1 and TS1/TS3 might be the result of compensation between two contrary effects: SST bias correction on the one hand, and the lack of SST feedback and variability on the other hand.

Moving to the impact of the regional SST anomalies prescribed in TS4 and TS5, the results indicate significant sensitivity of the future Indian summer monsoon.

(i) Increasing the SST anomalies in the southern high latitudes, where the deficit of sea ice in the present-day CCM climatology could lead actually to a strong underestimation of the surface warming in SG1, has a limited but not negligible impact on the monsoon response to increased concentrations of GHG. The precipitation increase relative to the present-day climate (TS1) is weaker than in TS3, especially in the northwest and south of the Indian subcontinent. Such a remote impact could be due to a perturbation of the regional Hadley circulation through a meridional propagation of the high-latitudes anomalies.

(ii) Prescribing zonal mean instead of El Niño-like SST anomalies in the tropical Pacific has a stronger influence on the monsoon response, with a large decrease in monsoon rainfall over much of South Asia relative to TS3, which fully cancels the precipitation increase caused by the global warming. In this case, it seems that a regional perturbation of the Walker circulation is mainly responsible for the impact.

(iii) In both sensitivity experiments, the prescribed regional SST anomalies, though limited in their extent and magnitude, induce significant perturbations in the Indian monsoon circulation and precipitation as large as the impact of increased concentrations of GHG.

These results provide some possible explanations for the lack of consensus about the Indian monsoon response in the IPCC scenarios (Houghton et al. 2001). Coupled climate models still show serious deficiencies in simulating the present-day climate in both tropical and high-latitude regions. They also provide contrasting SST anomalies in response to increasing amounts of GHG, notably in the southern high latitudes and in the tropical Pacific. The large sensitivity of the ARPEGE AGCM to “reasonable” perturbations of the late twenty-first-century SSTs in these regions suggests that such uncertainties should be strongly reduced before the global modeling community can provide more reliable climate projections over South Asia and possibly other regions. Beyond the important issue of downscaling the impacts of global warming at the regional scale, further work is urgently needed to better predict the large-scale consequences of the anthropogenic emissions of GHG. However, note that this rather pessimistic conclusion must be tempered. The strong sensitivity to regional SST uncertainties found in our time-slice simulations might be overestimated because of the lack of SST feedback in such experiments. Douville (2005) showed recently that neglecting this feedback has a significant impact on the atmospheric sensitivity to global warming and to interannual SST variability. More robust conclusions could be drawn through the coupling of the ARPEGE AGCM with a slab ocean model relaxed toward a prescribed SST climatology, an experiment we would like to carry out in the near future.

Acknowledgments. This study is part of an Indo-French collaboration project supported by a grant from the Indo-French Centre for the Promotion of Advanced Research (Project Number 2407-1). The authors are thankful to the Director of CNRM and the Director of IITM for encouraging this collaboration.

Thanks are also due to J.-F. Royer for helpful discussions, Brian Doty for developing the GrADS software, and the anonymous reviewers for their constructive comments.

REFERENCES

- Ashrit, R. G., H. Douville, and K. Rupa Kumar, 2003: Response of the Indian monsoon and ENSO–monsoon teleconnection to enhanced greenhouse effect in the CNRM coupled model. *J. Meteor. Soc. Japan*, **81**, 779–803.
- Boucher, O., and U. Lohman, 1995: The sulfate-CCN-cloud albedo effect: A sensitivity study with two general circulation models. *Tellus*, **47**, 281–300.
- Bougeault, P., 1985: A simple parameterization of the large-scale effects of cumulus convection. *Mon. Wea. Rev.*, **113**, 2108–2121.
- Camberlin, P., Y. Zhao, F. Chauvin, and H. Douville, 2004: Simulated ENSO-tropical rainfall teleconnections as from the ARPEGE-OPA coupled ocean-atmosphere model. *Climate Dyn.*, **23**, 641–657.
- Déqué, M., C. Drevet, A. Braun, and C. Cariolle, 1994: The ARPEGE/IFS atmospheric model, a contribution to French Community climate modelling. *Climate Dyn.*, **10**, 249–266.
- , P. Marquet, and R. G. Jones, 1998: Simulation of climate change over Europe using a global variable resolution general circulation model. *Climate Dyn.*, **14**, 173–189.
- Douville, H., 2005: Limitations of time-slice experiments for predicting climate change over South Asia. *Climate Dyn.*, **24**, 373–391.
- , J.-F. Royer, and J.-F. Mahfouf, 1995a: A new snow parameterization for the Météo-France climate model. Part-I: Validation in stand-alone experiments. *Climate Dyn.*, **12**, 21–35.
- , —, and —, 1995b: A new snow parameterization for the Météo-France climate model. Part-II: Validation in a 3D GCM experiment. *Climate Dyn.*, **12**, 37–52.
- , S. Planton, J.-F. Royer, D. B. Stephenson, S. Tyteca, L. Kergoat, S. Lafont, and R. A. Betts, 2000a: Importance of vegetation feedbacks in doubled-CO₂ climate experiments. *J. Geophys. Res.*, **105**, 14 841–14 861.
- , J.-F. Royer, J. Polcher, P. Cox, N. Gedney, D. B. Stephenson, and P.-J. Valdes, 2000b: Impact of CO₂ doubling on the Asian summer monsoon: Robust versus model dependent responses. *J. Meteor. Soc. Japan*, **78**, 1–19.
- , F. Chauvin, S. Planton, J.-F. Royer, D. Salas Méliá, and S. Tyteca, 2002: Sensitivity of the hydrological cycle to increasing amounts of greenhouse gases and aerosols. *Climate Dyn.*, **20**, 45–68.
- Gadgil, S., and S. Sajani, 1998: Monsoon precipitation in the AMIP runs. *Climate Dyn.*, **14**, 659–689.
- Hu, Z.-Z., M. Latif, E. Roeckner, and L. Bengtsson, 2000: Intensified Asian summer monsoon and its variability in a coupled model forced by increasing greenhouse gas concentrations. *Geophys. Res. Lett.*, **27**, 2681–2684.
- Huffman, G. J., and Coauthors, 1997: The Global Precipitation Climatology Project (GPCP) combined precipitation dataset. *Bull. Amer. Meteor. Soc.*, **78**, 5–20.
- Houghton, J. T., Y. Ding, D. J. Griggs, M. Noguer, P. J. van der Linden, and D. Xiaosu, Eds., 2001: *Climate Change 2001: The Scientific Basis*. Cambridge University Press, 944 pp.
- Kitoh, A., and O. Arakawa, 1999: On overestimation of tropical precipitation by an atmospheric GCM with prescribed SST. *Geophys. Res. Lett.*, **26**, 2965–2968.
- , S. Yukimoto, A. Noda, and T. Motoi, 1997: Simulated changes in the Asian summer monsoon at times of increased atmospheric CO₂. *J. Meteor. Soc. Japan*, **75**, 1019–1031.
- Krishna Kumar, K., M. Hoerling, and B. Rajagopalan, 2005: Advancing dynamical prediction of Indian monsoon rainfall. *Geophys. Res. Lett.*, **32**, L08704, doi:10.1029/2004GL021979.
- Lal, M., U. Cubasch, and B. D. Santer, 1994: Effect of global warming on Indian monsoon simulated with a coupled ocean-atmosphere general circulation model. *Curr. Sci.*, **66**, 430–438.
- , —, R. Voss, and J. Waszkewitz, 1995: Effect of transient increase in greenhouse gases and sulfate aerosols on monsoon climate. *Curr. Sci.*, **69**, 752–763.
- Levitus, S., 1982: *Climatological Atlas of the World Ocean*. NOAA Prof. Paper 13, 173 pp. and 17 microfiche.
- Louis, J.-F., M. Tiedtke, and J.-F. Geleyn, 1982: A short history of the operational PBL-parameterization at ECMWF. *Proc. ECMWF Workshop on Planetary Boundary Layer Parameterization*, Reading, United Kingdom, ECMWF, 59–88.
- Madec, G., P. Delecluse, M. Imbrad, and C. Levy, 1997: OPA version 8.0 Ocean General Circulation Model reference manual. LODYC Int. Rep. 97/04, 141 pp. [Available from Laboratoire d’Océanographie Dynamique et de Climatologie, Université Paris VI, Paris 7525, France.]
- Meehl, G. A., and W. M. Washington, 1993: South-Asian summer monsoon variability in a model with doubled atmospheric carbon dioxide concentration. *Science*, **260**, 1101–1104.
- , W. D. Collins, B. A. Boville, J. T. Kiehl, T. M. L. Wigley, and J. M. Arblaster, 2000: Response of the NCAR climate system model to increased CO₂ and the role of physical processes. *J. Climate*, **13**, 1879–1898.
- Menendez, C. G., V. Serafini, and H. Le Treut, 1999: The effect of sea ice on the transient atmospheric eddies of the Southern Hemisphere. *Climate Dyn.*, **15**, 659–671.
- Mitchell, J. F. B., and C. A. Senior, 1989: The antarctic winter; simulations with climatological and reduced sea ice extents. *Quart. J. Roy. Meteor. Soc.*, **115**, 225–246.
- , and T. C. Johns, 1997: On modification of global warming by sulfate aerosols. *J. Climate*, **10**, 245–267.
- Morcrette, J. J., 1989: Description of radiative scheme in the ECMWF model. ECMWF Tech. Memo. 165, 26 pp.
- , 1990: Impact of changes to the radiative transfer parameterizations plus cloud optical properties in the ECMWF model. *Mon. Wea. Rev.*, **118**, 847–873.
- Noilhan, J., and J. F. Mahfouf, 1996: The ISBA land surface parameterization scheme. *Global Planet. Change*, **13**, 145–159.
- Pant, G. B., and K. Rupa Kumar, 1997: *Climates of South Asia*. John Wiley & Sons, 320 pp.
- Penner, J. E., C. C. Chuang, and K. Grant, 1998: Climate forcing by carbonaceous and sulfate aerosols. *Climate Dyn.*, **14**, 839–851.
- Ricard, J.-L., and J.-F. Royer, 1993: A statistical cloud scheme for use in a AGCM. *Ann. Geophys.*, **11**, 1095–1115.
- Royer, J. F., and Coauthors, 2002: Simulation of climate change during the 21st century including stratospheric ozone. *C. R. Geosci.*, **334**, 147–154.
- Rupa Kumar, K., and R. G. Ashrit, 2001: Regional aspects of global climate change simulations: Validation and assessment of climate response over Indian monsoon region to transient increase of greenhouse gases and sulfate aerosols. *Mausam*, **52**, 229–244.

- , G. B. Pant, B. Parthasarathy, and N. A. Sontakke, 1992: Spatial and subseasonal patterns of the long-term trends of Indian summer monsoon rainfall. *Int. J. Climatol.*, **12**, 257–268.
- Salas Mélia, D., 2002: A global coupled sea ice-ocean model. *Ocean Modell.*, **4**, 137–172.
- Simmonds, I., and T. H. Jacka, 1995: Relationships between the interannual variability of Antarctic sea ice and the Southern Oscillation. *J. Climate*, **8**, 637–648.
- Stephenson, D. B., and I. M. Held, 1993: GCM response of northern winter stationary waves and storm tracks to increasing amounts of carbon dioxide. *J. Climate*, **6**, 1859–1870.
- Timmermann, A., J. Oberhuber, A. Bacher, M. Esch, M. Latif, and E. Roeckner, 1999: Increased El Niño frequency in a climate model forced by future greenhouse warming. *Nature*, **398**, 694–697.
- Wang, B., R. Wu, and K. M. Lau, 2001: Interannual variability of the Asian summer monsoon: Contrasts between the Indian and the Western North Pacific–East Asian monsoons. *J. Climate*, **14**, 4073–4090.
- Yu, B., and G. B. Boer, 2002: The roles of radiation and dynamical processes in the El Niño-like response to global warming. *Climate Dyn.*, **19**, 539–553.
- Yuan, X., and D. G. Martinson, 2000: Antarctic sea ice extent variability and its global teleconnectivity. *J. Climate*, **13**, 1697–1717.